Since January 2020 Elsevier has created a COVID-19 resource centre with free information in English and Mandarin on the novel coronavirus COVID-19. The COVID-19 resource centre is hosted on Elsevier Connect, the company's public news and information website.

Elsevier hereby grants permission to make all its COVID-19-related research that is available on the COVID-19 resource centre - including this research content - immediately available in PubMed Central and other publicly funded repositories, such as the WHO COVID database with rights for unrestricted research re-use and analyses in any form or by any means with acknowledgement of the original source. These permissions are granted for free by Elsevier for as long as the COVID-19 resource centre remains active.

Cell

Identification of Oxidative Stress and Toll-like Receptor 4 Signaling as a Key Pathway of Acute Lung Injury

Yumiko Imai,[1,16,*] Keiji Kuba,[1,2] G. Greg Neely,[1] Rubina Yaghubian-Malhami,[1] Thomas Perkmann,[3] Geert van Loo,[4] Maria Ermolaeva,[4,5] Ruud Veldhuizen,[6] Y.H. Connie Leung,[8] Hongliang Wang,[9] Haolin Liu,[9] Yang Sun,[9] Manolis Pasparakis,[4,5] Manfred Kopf,[10] Christin Mech,[11] Sina Bavari,[11] J.S. Malik Peiris,[8] Arthur S. Slutsky,[12,13] Shizuo Akira,[14] Malin Hultqvist,[15] Rikard Holmdahl,[15] John Nicholls,[7] Chengyu Jiang,[9] Christoph J. Binder,[3] and Josef M. Penninger[1,*]

[1]IMBA, Institute of Molecular Biotechnology of the Austrian Academy of Sciences, Dr. Bohrgasse 3, A-1030 Vienna, Austria
[2]Medical Research Institute, Tokyo Medical and Dental University, Kandasurugadai 2-3-10, Chiyoda-ku, Tokyo 101-0062, Japan
[3]CeMM, Research Center for Molecular Medicine of the Austrian Academy of Sciences and Institute of Medical and Chemical Laboratory Diagnostics, Medical University of Vienna, Währinger Gürtel 18-20, A-1090 Vienna, Austria
[4]European Molecular Biology Laboratory (EMBL), Mouse Biology Unit, Via Ramarini 32, Monterotondo-Scalo, Rome 00016, Italy
[5]Institute for Genetics, University of Cologne, Zülpicher Str. 47, D-50674 Cologne, Germany
[6]Lawson Health Research Institute, Departments of Medicine and Physiology and Pharmacology, The University of Western Ontario, London Ontario, N6A 4V2, Canada
[7]Department of Pathology
[8]Department of Microbiology
University of Hong Kong, SAR
[9]National Key Laboratory of Medical Molecular Biology, School of Basic Medicine Peking Union Medical College and Chinese Academy of Medical Sciences, Beijing 100005, China
[10]Molecular Biomedicine, Swiss Federal Institute of Technology, Wagistrasse 27, CH-8952 Zürich-Schlieren, Switzerland
[11]US Army Medical Research Institute of Infectious Diseases, Fort Detrick, Frederick, MD 21701, USA
[12]Interdepartmental Division of Critical Care Medicine
[13]Department of Critical Care, St. Michael's Hospital
University of Toronto, Toronto M5B 1W8, Canada
[14]Department of Host Defense, Research Institute for Microbial Diseases, Osaka University, Osaka 565-0871, Japan
[15]Medical Inflammation Research, MBB, Karolinska Institutet, Stockholm, Sweden and Medical Inflammation Research BMC I11 Lund, Sweden
[16]Present address: The Global COE program, Akita University School of Medicine, Akita 010-8543, Japan.
*Correspondence: josef.penninger@imba.oeaw.ac.at (J.M.P.), imai@med.akita-u.ac.jp (Y.I.)
DOI 10.1016/j.cell.2008.02.043

SUMMARY

Multiple lung pathogens such as chemical agents, H5N1 avian flu, or SARS cause high lethality due to acute respiratory distress syndrome. Here we report that Toll-like receptor 4 (TLR4) mutant mice display natural resistance to acid-induced acute lung injury (ALI). We show that TLR4-TRIF-TRAF6 signaling is a key disease pathway that controls the severity of ALI. The oxidized phospholipid (OxPL) OxPAPC was identified to induce lung injury and cytokine production by lung macrophages via TLR4-TRIF. We observed OxPL production in the lungs of humans and animals infected with SARS, Anthrax, or H5N1. Pulmonary challenge with an inactivated H5N1 avian influenza virus rapidly induces ALI and OxPL formation in mice. Loss of TLR4 or TRIF expression protects mice from H5N1-induced ALI. Moreover, deletion of *ncf1,* which controls ROS production, improves the severity of H5N1-mediated ALI. Our data identify oxidative stress and innate immunity as key lung injury pathways that control the severity of ALI.

INTRODUCTION

In 2003, severe acute respiratory syndrome (SARS) spread rapidly from China throughout Asia to Canada (World Health Organization, 2008). Most patients who died of SARS developed acute respiratory distress syndrome (ARDS) (Lew et al., 2003)—the most severe form of acute lung injury (ALI) (Ware and Matthay, 2000). ARDS was also the cause of death in millions of people during the Spanish Influenza pandemic (Tumpey et al., 2005). Recently, H5N1 avian influenza virus infections have spread through the world primarily infecting poultry and migratory birds. The reported death rates of H5N1 avian influenza infections in humans are ~50%, prompting the fear that H5N1 might cause a worldwide pandemic (Beigel et al., 2005; World Health Organization, 2005).

The high lethality of H5N1 or SARS infections as well as their economic and social impact makes it paramount to explore common disease mechanisms and novel therapeutic targets of ARDS. Moreover, many viruses including H5N1 mutate readily

and produce resistant strains that are no longer controlled by vaccines or antiviral drugs. The pathology of ARDS in SARS-coronavirus (Lew et al., 2003) and H5N1 avian influenza virus infections (Beigel et al., 2005; Peiris et al., 2004) is characterized by accumulation of inflammatory cells, edema formation, and a marked increase in cytokines. The same clinical syndrome of acute lung failure is observed in multiple other pathogenic conditions including sepsis, gastric acid aspiration, or pulmonary infections with Anthrax spores (Hudson et al., 1995; Guarner et al., 2003). Similar ARDS symptoms can be observed in multiple species ranging from birds, rodents, tigers, and primates to humans. Given the common pathology, we wondered whether there might be a conserved injury pathway for ARDS.

RESULTS

TLR4 Is a Susceptibility Gene for ALI

To identify endogenous genes that control the severity of ALI, we tested inbred mouse strains for their propensity to develop ALI in response to acid aspiration, a model that recapitulates the acute phase of human ARDS (Imai et al., 2005; Nagase et al., 2000). Acid aspiration in mice results in rapid impairment of lung function as determined by increased lung elastance, a measure of the change in pressure achieved per unit change in volume, representing the stiffness of the lungs, decreased blood oxygenation, and alveolar wall thickening, bleeding, inflammatory cell infiltration, and formation of hyaline membranes (Figures S1A–S1C available online). The severity of acid-induced ALI was comparable among various inbred mouse strains with one exception: C3H/HeJ mice exhibited reduced lung elastance. Moreover, C3H/HeJ mice exhibited better blood oxygenation and reduced inflammation (Figures S1A–S1C).

C3H/HeJ mice exhibit resistance to a lipopolysaccharide (LPS) challenge due to a mutation in the intracellular domain of Toll-like receptor 4 (TLR4) ($Tlr4^{Lps\text{-}d}$) that interferes with TLR4 signaling (Poltorak et al., 1998). To test whether this TLR4 mutation might be involved in ALI severity, we assessed acid-induced ALI in C3H/HeOuJ mice, a C3H-congenic mouse strain that expresses wild-type (WT) TLR4. The resistance to ALI of C3H/HeJ mice was lost in C3H/HeOuJ mice (Figures S1A–S1D). To confirm that TLR4 determines disease severity, we triggered acid-mediated ALI in $tlr4^{-/-}$ mice (Hoshino et al., 1999). Genetic inactivation of *tlr4* markedly attenuated ALI as determined by improved lung elastance (Figure 1A), reduced edema formation (Figure 1B), and ameliorated histological changes (Figure 1C). Bone marrow chimeras showed that the severity of ALI is controlled by TLR4 expression on hematopoietic cells (Figures 1D–1F). Lung pathology were not affected in *tlr3* (Yamamoto et al., 2003) or *tlr9* (Hemmi et al., 2000) mutant mice (Figures S2A and S2B). These data identify TLR4 as a susceptibility gene for ALI.

Acute Lung Injury Is Mediated via TLR4-TRIF-TRAF6-NF-κB Signaling

TLR4 stimulation is relayed to cellular responses via different adaptors such as MyD88 and TRIF (Akira et al., 2006). Surprisingly, genetic deletion of *myd88* (Adachi et al., 1998) had no apparent effect on the severity of ALI (Figures S2C and S2D). In contrast, $trif^{-/-}$ mice (Yamamoto et al., 2003) exhibited markedly improved lung function (Figure 2A), lung pathology (Figure 2B), and lung edema (Figure S3A). TRIF signals either through IKK-ε and activation of IRF3 or via TRAF6-mediated NF-κB activation (Sato et al., 2003). To dissect the TLR4-TRIF activation pathway, we conducted experiments using *irf3* and *traf6* knockout mice. Deletion of *irf3* (Sato et al., 2000) did not show a significant change in acid-mediated ALI (Figures S2E and S2F). We next generated myeloid cell-specific *traf6* mutant mice using Lys-Cre-mediated deletion of a $TRAF6^{flox/flox}$ allele ($TRAF6^{MC\text{-}KO}$). Deletion of TRAF6 was confirmed in cultured bone marrow-derived macrophages (Figure 2C). Inactivation of TRAF6 in $TRAF6^{MC\text{-}KO}$ mice resulted in alleviation of ALI (Figures 2D, 2E, and S3B). To determine whether mutations of TLR4, TRIF, or TRAF6 affect NF-κB activation, we performed in situ signaling experiments to detect nuclear accumulation of Ser276-phosphorylated NF-κBp65 indicative of NF-κB activation (Vermeulen et al., 2002). Whereas acid aspiration triggered NF-κBp65 activation in WT and $myd88^{-/-}$ mice, much less nuclear NF-κBp65 translocation occurred in lungs from $tlr4^{-/-}$, $trif^{-/-}$, or $TRAF6^{MC\text{-}KO}$ mice (Figure 2F). NF-κB activation was largely restricted to macrophages. Taken together, our genetic results identify TLR4-TRIF-TRAF6-NF-κB as a key signaling pathway that links acid injury to the severity of ALI.

IL-6 Mediates Acute Lung Injury

Local cytokine production at the site of injury is one of the hallmarks of ALI (Martin, 1999). The molecular basis of how such cytokine storms are mediated by local injury and whether such injury-released cytokines actually contribute to disease severity of ARDS are still unknown. To examine whether TLR4 signaling may be involved in local cytokine, we performed multiple cytokine arrays from normal lungs and lung tissue following acid aspiration. The cytokines IL-6, IL-1β, and KC (IL-8) were upregulated by acid treatment in WT mice, but we failed to observe upregulation of TNFα, IL-2, IFN-γ, IL-1α, IL-12p40, IL-12p70, IL-17, RANTES, IL-9, Eotaxin, or MIP-1β (Figure S4 and data not shown). IL-3, IL-4, IL-5, IL-13, G-CSF, GM-CSF, MCP-1, and MIP-1α were below the detection limit of our assay. IL-10 negatively correlated with the severity of ALI (Figure S4E). In particular, IL-6 levels closely reflected the severity of ALI in resistant $tlr4^{-/-}$, $trif^{-/-}$, and $TRAF6^{MC\text{-}KO}$ mice and injury-prone mice $myd88^{-/-}$ and $irf3^{-/-}$ mice (Figure 2G). To test if IL-6 is indeed involved in the pathogenesis of ALI, we studied $il\text{-}6^{-/-}$ mice (Kopf et al., 1994). In response to acid aspiration, $il\text{-}6^{-/-}$ mice exhibited significant improvement of lung function (Figure 2H), lung edema formation (Figure S3C), and decreased lung pathologies (Figure 2I). Although these data do not exclude the importance of other cytokines, our genetic results show that loss of IL-6 alleviates the severity of ALI (Figure 2J).

Oxidative Stress and Formation of Oxidized Phospholipids in ALI

Since we used acid aspiration to trigger ALI, a key question emerged: what triggers TLR4 under such injury conditions? To rule out the possibility of LPS contamination, we first treated mice with polymyxin B to neutralize LPS (Jacobs and Morrison, 1977). Polymyxin B did not alter disease severity in acid-induced ALI (Figure S5A). Moreover, in line with previous data from our

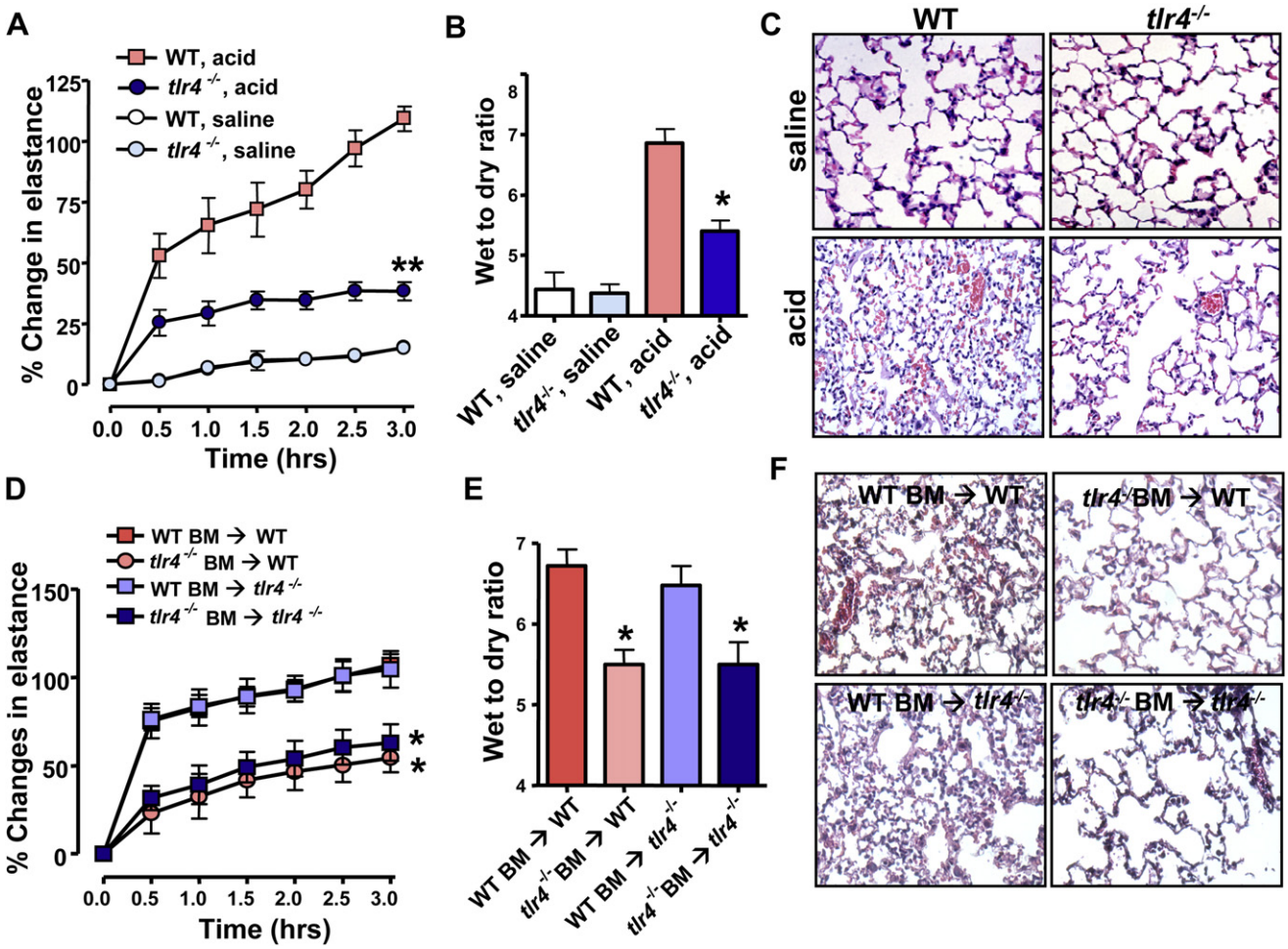

Figure 1. TLR4 Is a Susceptibility Gene for Acute Lung Injury

(A) Changes in lung elastance after acid or saline treatment in WT and *tlr4*$^{-/-}$ mice. n = 8–10 for acid-treated groups, n = 6 for saline-treated groups. **p < 0.01 for the whole time course.

(B) Lung edema formation after acid or saline treatment. *p < 0.05.

(C) Lung histopathology. H&E staining. Original magnifications × 200.

(D) Lung elastance after acid treatment of WT mice transplanted with WT bone marrow (BM) (WT BM → WT), WT mice receiving *tlr4*$^{-/-}$ BM (*tlr4*$^{-/-}$ BM → WT), *tlr4*$^{-/-}$ mice transplanted with WT BM (WT BM → *tlr4*$^{-/-}$), and *tlr4*$^{-/-}$ mice receiving *tlr4*$^{-/-}$ BM (*tlr4*$^{-/-}$ BM → *tlr4*$^{-/-}$). n = 6 for each group.

(E) Lung edema formation and (F) lung histopathology 3 hr after acid injury in WT BM → WT, *tlr4*$^{-/-}$ BM → WT, WT BM → *tlr4*$^{-/-}$, and *tlr4*$^{-/-}$ BM → *tlr4*$^{-/-}$ chimeras.

In (D) and (E), *p < 0.05 comparing WT BM → WT or WT BM → *tlr4*$^{-/-}$ mice. n = 6 for each group. H&E staining. Original magnifications × 200. Data in (A), (B), (D), and (E) are mean values ± SEM.

group (Imai et al., 2005) and others (Nagase et al., 2000), instillation of LPS alone into lungs does not worsen lung function in our acute lung failure model (Figure S5B). We next stimulated alveolar macrophages from WT, *tlr4*$^{-/-}$, *myd88*$^{-/-}$, or *trif*$^{-/-}$ mice with bronchoalveolar lavage (BAL) fluid from normal mice (BAL control), BAL fluid from lungs of acid-treated WT mice (BAL acid), or LPS. In line with our genetic data, BAL fluid-induced IL-6 production was mediated via TLR4 and TRIF, but not MyD88 (Figure 3A). By contrast, LPS-induced IL-6 production in alveolar macrophages was dependent on TLR4, MyD88, and TRIF (Figure 3A). Thus, other TLR4-activating agents rather than LPS are generated during the course of ALI.

Since the lung air-liquid interface is exposed to the aerobic environment and therefore susceptible to oxidation, we speculated that ALI could result from the local generation of reactive oxygen species (ROS) and the subsequent formation of oxidized phospholipids (OxPLs). We indeed observed induction of ROS in alveolar macrophages following in vivo acid challenge (Figure 3B). Acid treatment also triggered enhanced TLR4 surface expression (Figure 3C). To demonstrate the role of OxPLs in vivo we used the well-characterized mAb EO6 (Friedman et al., 2002). This mAb specifically detects the phosphocholine (PC) headgroup of phospholipids in which the sn2 side chain has been oxidized but does not recognize native nonoxidized PLs. We

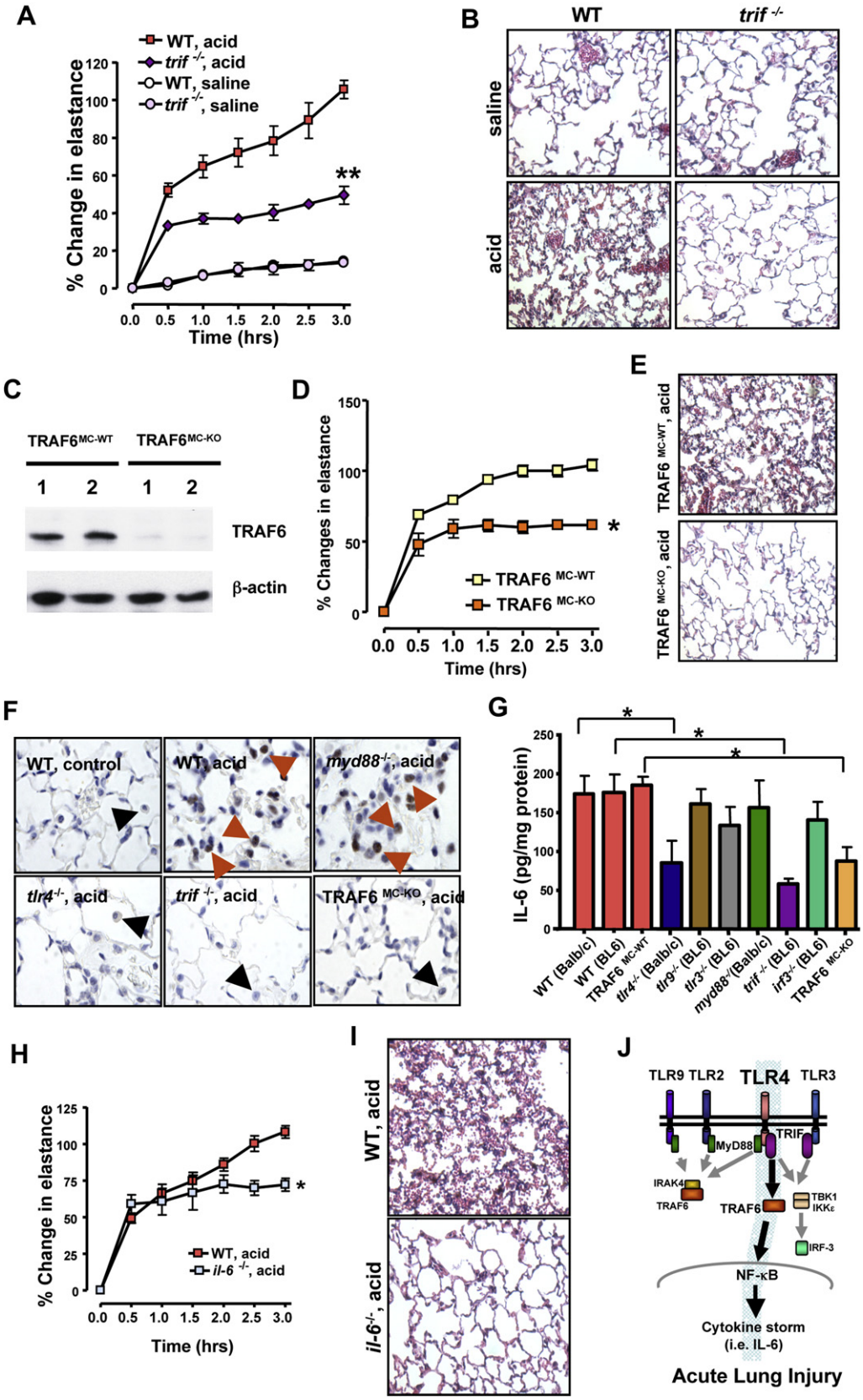
A
WT, acid
trif -/-, acid
WT, saline
trif -/-, saline
% Change in elastance
Time (hrs)
**
B
WT
trif -/-
saline
acid
C
TRAF6MC-WT
TRAF6MC-KO
1 2 1 2
TRAF6
β-actin
D
% Changes in elastance
Time (hrs)
TRAF6 MC-WT
TRAF6 MC-KO
*
E
TRAF6 MC-WT, acid
TRAF6 MC-KO, acid
F
WT, control
WT, acid
myd88-/-, acid
tlr4-/-, acid
trif -/-, acid
TRAF6 MC-KO, acid
G
IL-6 (pg/mg protein)
WT (Balb/c)
WT (BL6)
TRAF6 MC-WT
tlr4-/- (Balb/c)
tlr9-/- (BL6)
tlr3-/- (BL6)
myd88-/-(Balb/c)
trif -/- (BL6)
irf3-/- (BL6)
TRAF6 MC-KO
H
% Change in elastance
Time (hrs)
WT, acid
il-6 -/-, acid
*
I
WT, acid
il-6-/-, acid
J
TLR9 TLR2
TLR4
TLR3
MyD88
TRIF
IRAK4
TRAF6
TRAF6
TBK1
IKKε
IRF-3
NF-κB
Cytokine storm
(i.e. IL-6)
Acute Lung Injury

observed large amounts of EO6-detectable OxPLs in the BAL fluid of acid-challenged animals (Figure S5C). In situ immunohistochemistry confirmed the generation of EO6-detectable OxPLs in alveolar macrophages as well as inflammatory exudates lining the injured air spaces (Figure 3D). In addition, we observed formation of the lipid peroxidation breakdown product malondialdehyde detected by the specific mAb MDA2 (Palinski et al., 1996) (Figure S5D), further confirming that lipid oxidation does occur in diseased lungs. These data show that acid aspiration triggers the oxidative stress machinery and the generation of OxPLs in lung.

OxPLs Induce Cytokine Production and Acute Lung Injury via TLR4

Minimally modified low-density lipoprotein (LDL) has been previously shown to mediate macrophage activation (Miller et al., 2003a, 2005) and to modulate the severity of atherosclerosis and inflammatory responses via TLR4 (Miller et al., 2003a; Michelsen et al., 2004). To address whether OxPLs generated during ALI can activate innate immune responses, we stimulated WT and *tlr4*$^{-/-}$ alveolar macrophages with BAL fluid from normal (BAL control) and diseased lungs (BAL acid). BAL fluid from mice with ALI, which contains OxPLs (Figure S5C), induced large amounts of IL-6 production in WT alveolar macrophages. Neutralization of OxPLs by the specific mAb EO6 attenuated BAL fluid-induced IL-6 production (Figure 3E). BAL fluid did not trigger IL-6 release in *tlr4*$^{-/-}$ alveolar macrophages (Figure 3E). Similarly, BAL fluid from diseased mice induced IL-6 production in peritoneal (Figure S6A) and bone marrow macrophages (Figure S6B), which was reverted by EO6 Ab treatment. Induction of IL-6 was again dependent on TLR4 expression (Figures S6A and S6B). OxPLs were also observed in acid-treated *trl4*$^{-/-}$ mice (Figure S6C).

The major source of PLs in the lung is surfactant, which forms a film at the alveolar air-water interface and reduces surface tension. Surfactant contains 80%–90% PLs including unsaturated phosphatidylcholine that can be oxidized (Rodriguez Capote et al., 2003; Veldhuizen et al., 1998). In vitro-oxidized surfactant PLs contain EO6-detectable OxPLs (Figure S6D). Addition of purified synthetically oxidized surfactant PLs induced IL-6 production in a dose-dependent manner in WT peritoneal macrophages (Figure 3F). IL-6 production in response to surfactant OxPLs was decreased by the neutralizing mAb EO6 (data not shown) and dependent on TLR4 expression (Figure 3F). In line with previous results (Bailey et al., 2004), in vivo administration of nonoxidized PLs induces slightly impaired lung function (Figure 3G). Intratracheal administration of OxPLs markedly worsened lung function in normal mice (Figure 3G). In a second experimental model, we removed endogenous surfactant via saline lavages, which strongly impairs lung function; we followed this with intratracheal replacement with nonoxidized or oxidized surfactant PLs. In this scenario, challenge with OxPLs resulted in much more severe impairment of lung function and all experimental animals died by 2 hr, whereas mice that received control, nonmodified surfactant PLs stabilized their lung function (Figure S7A). Lung function was comparable among WT and *tlr4*$^{-/-}$ mice following administration of nonoxidized surfactant PLs. Loss of TLR4 expression markedly alleviated the severe lung failure phenotype following OxPLs treatment (Figure 3H). Moreover, administration of OxPLs induced increased levels of IL-6 in the lungs of WT control but not in those of *tlr4*$^{-/-}$ mice (Figure S7B). These data indicate that synthetically oxidized surfactant PLs can trigger cytokine production in macrophages and, importantly, acute lung injury in vivo via TLR4.

OxPAPC Triggers Acute Lung Injury

We next attempted to identify specific OxPLs that can trigger ALI via TLR4. The mAb EO6 we used for the detection of OxPLs has been previously reported to specifically bind PC-containing OxPLs such as oxidized 1-palmitoyl-2-arachidonoyl-phosphatidylcholine (OxPAPC) (Figure S7C). We confirmed that the mAB EO6 indeed detects OxPAPC (Figure S8A). To directly test whether OxPAPC can trigger cytokine production via TLR4, we stimulated lung tissue macrophages with OxPAPC and nonoxidized PAPC. Compared to PAPC, OxPAPC induced higher IL-6 levels in WT macrophages, and these levels were attenuated by the neutralizing mAb EO6 (Figure 4A). OxPAPC-induced IL-6 production was decreased in *tlr4*$^{-/-}$ and *trif*$^{-/-}$ lung macrophages, and this residual IL-6 production was not affected by the mAb EO6 (Figure 4B). Similar to our in vivo experiments, OxPAPC

Figure 2. TRIF-TRAF6-NFκB-Cytokine Signaling Mediates the Severity of Acid Aspiration-Induced Acute Lung Injury

(A) Lung elastance after acid or saline treatment of WT and *trif*$^{-/-}$ mice. n = 6–10 for acid-treated groups, n = 4 for saline-treated groups. **p < 0.01 for the whole time course.

(B) Reduced inflammation and hyaline membrane formation in acid-treated *trif*$^{-/-}$ mice. H&E staining. Original magnifications × 200.

(C) TRAF6 protein expression in bone marrow macrophages isolated from Lys-Cre(–) TRAF6$^{flox/flox}$ (TRAF6^{MC-WT}) and Lys-Cre(+) TRAF6$^{flox/flox}$ (TRAF6^{MC-KO}) mice. β-actin protein is shown as control. Data from two different mice (1, 2) are shown for each genotype.

(D) Changes in lung elastance in TRAF6^{MC-WT} (n = 6) and TRAF6^{MC-KO} mice (n = 4) following acid aspiration. *p < 0.05 for the whole time course.

(E) Reduced inflammatory cell infiltration, bleeding, and hyaline membrane formation in acid-treated TRAF6^{MC-KO} mice. H&E staining. Original magnifications × 200.

(F) Immunolocalization of Ser276-phosphorylated NFκBp65 in lung tissue of saline-treated control WT mice and acid-treated WT, *myd88*$^{-/-}$ *tlr4*$^{-/-}$, *trif*$^{-/-}$, and TRAF6^{MC-KO} mice. Note the accumulation of phosphorylated NFκBp65 in nuclei of macrophages (red arrows) in acid-treated WT and *myd88*$^{-/-}$ mice, which is absent in lung macrophages (black arrows) from acid-treated *tlr4*$^{-/-}$, *trif*$^{-/-}$, and TRAF6^{MC-KO} mice. Original magnifications × 400.

(G) IL-6 levels in lung tissue after acid treatment in WT Balb/c, WT BL6, control TRAF6^{MC-WT} (wild-type), *tlr4*$^{-/-}$ (Balb/c background), *tlr9*$^{-/-}$ (BL6 background), *tlr3*$^{-/-}$ (BL6), *myd88*$^{-/-}$ (Balb/c) *trif*$^{-/-}$ (BL6), *irf3*$^{-/-}$ (BL6), and TRAF6^{MC-KO} mice. IL-6 levels were determined by whole lung tissue ELISA. n = 5–8 animals for each group. *p < 0.05.

(H) Lung elastance after acid treatment in interleukin-6 mutant (*il-6*$^{-/-}$) and control WT mice. n = 5–6 each group. *p < 0.05.

(I) Improved lung histopathology in acid-treated *il-6*$^{-/-}$ mice. H&E staining. Original magnifications × 200. Lungs were analyzed 3 hr after treatment.

(J) Schematic diagram depicting the role of TLR4 in ALI. Data in (A), (D), (G), and (H) are mean values ± SEM.

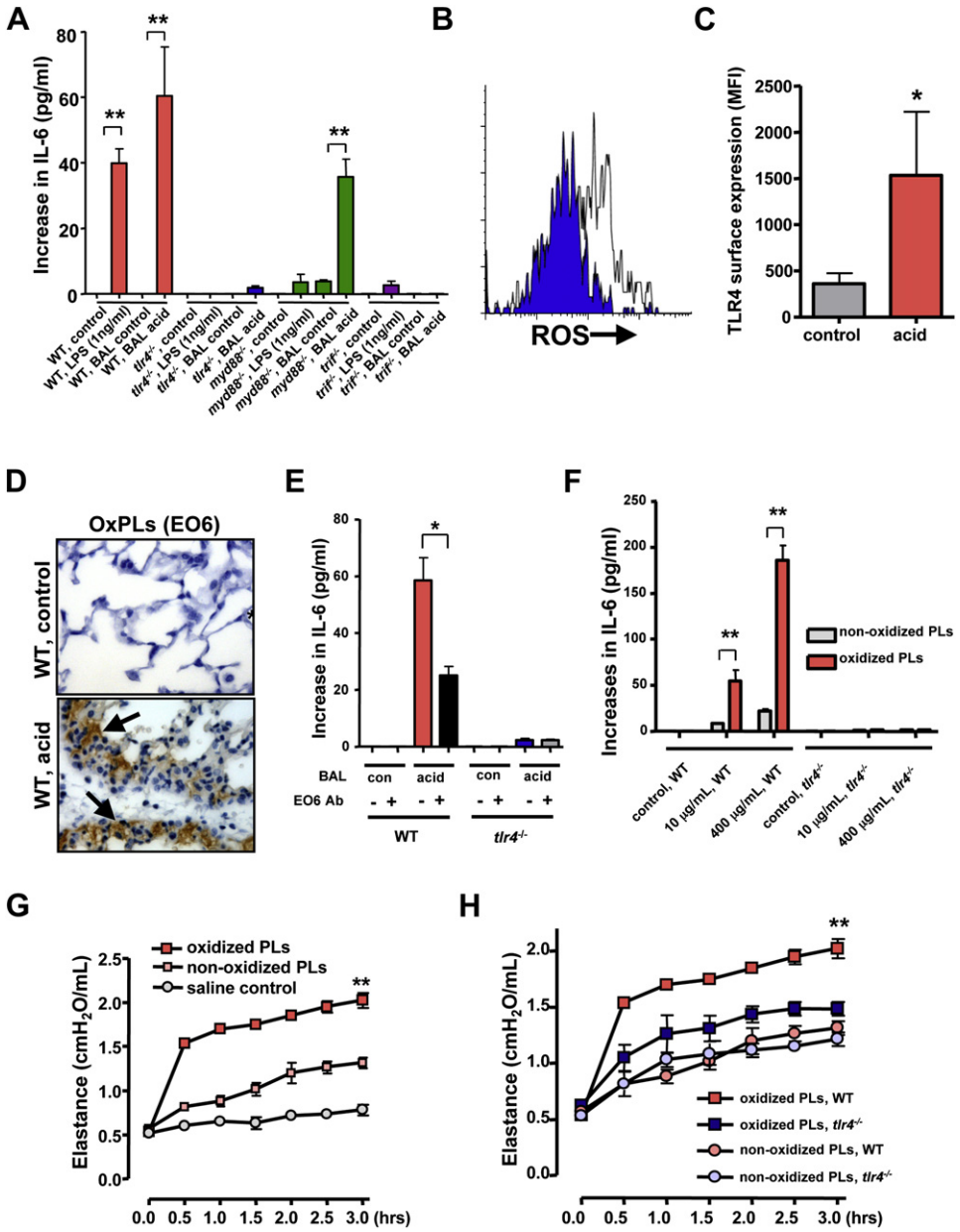

Figure 3. Formation of Oxidized Phospholipids in Acute Lung Injury

(A) Increase in IL-6 production from baseline in WT, *tlr4*$^{-/-}$, *myd88*$^{-/-}$, and *trif*$^{-/-}$ alveolar macrophages treated with LPS, BAL fluid from normal control, or BAL fluid from acid-treated WT mice. **p < 0.01. Data are from four separate experiments.

(B) Increases in ROS expression in alveolar macrophages obtained from WT mice 60 min after treatment with saline (background control, blue) or acid (white). A representative histogram is shown among five separate experiments.

(C) Increased TLR4 surface expression in alveolar macrophages from WT mice treated with saline (control) or acid. Data are from five separate experiments. *p < 0.05.

(D) Immunohistochemistry for OxPLs detected by the mAb EO6 in lungs of saline-treated control (upper panel) and acid-treated WT mice (lower panel). OxPLs were localized to inflammatory exudates lining the injured alveoli (arrows) in acid-treated lungs. Original magnifications × 400. Lungs were analyzed 3 hr after acid treatment.

(E) BAL fluid from acid-treated mice (BAL acid) induces large amounts of IL-6 in WT but not *tlr4*$^{-/-}$ alveolar macrophages. BAL fluid plus an isotype-matched control Ab was compared to BAL fluid plus the mAb EO6. *p < 0.05. Data are from four separate experiments.

(F) Increase in IL-6 from baseline in peritoneal macrophages isolated from WT and *tlr4*$^{-/-}$ mice in response to nonoxidized PLs or oxidized PLs. **p < 0.01.

(G) Lung elastance in WT mice following intratracheal administration of saline, nonoxidized PLs, and oxidized PLs. n = 4–6 for each group. **p < 0.01 for the whole time course.

(H) Lung elastance in WT and *tlr4*$^{-/-}$ mice following treatment with nonoxidized PLs or oxidized PLs. n = 4 for each group. **p < 0.01 for the whole time course. Data in (A), (C), and (E)–(H) are mean values ± SEM.

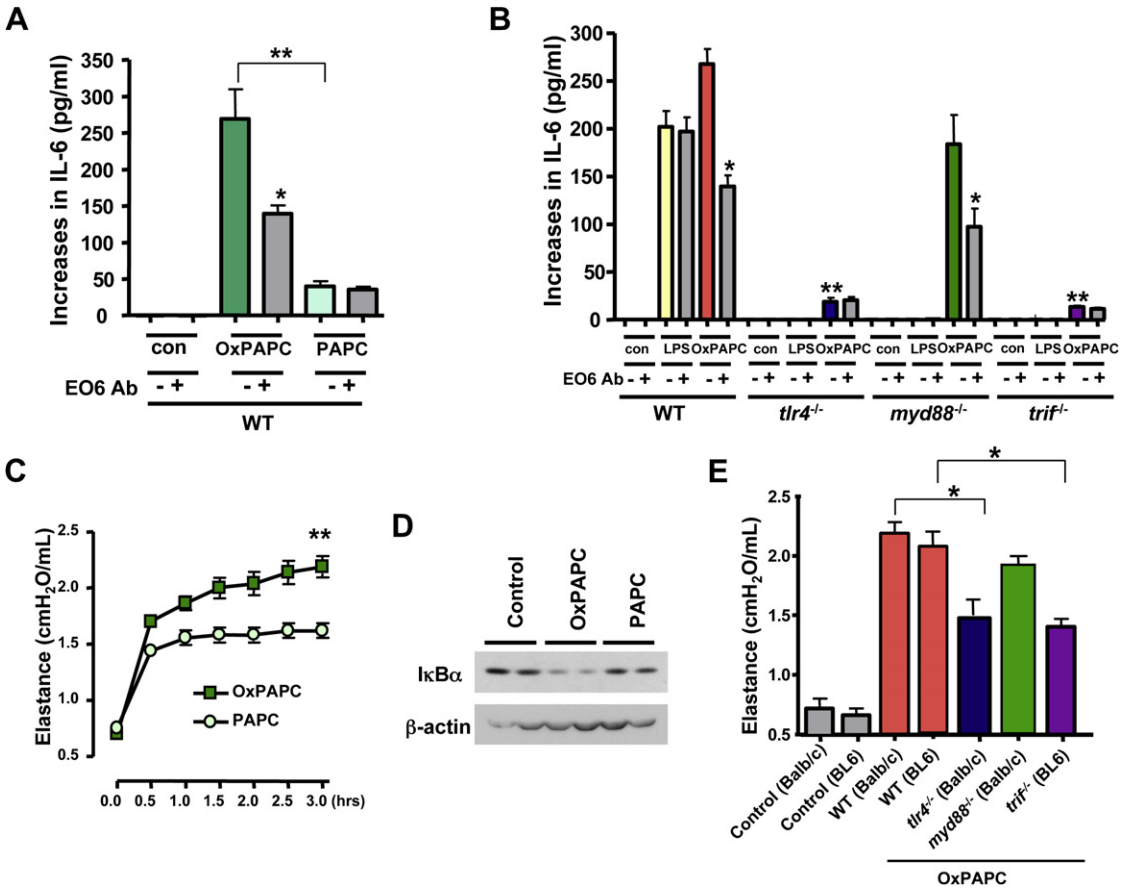

Figure 4. Oxidized PAPC Induces ALI and IL-6 Production via TLR4

(A) Increases in IL-6 production from baseline (unstimulated control) in lung tissue macrophages from WT mice in response to PAPC (10 μg/ml) or OxPAPC (10 μg/ml) in the presence of an isotype-matched control mAb or the mAb EO6. *$p < 0.05$ comparing mAb EO6(−). **$p < 0.01$ comparing OxPAPC EO6(−) and PAPC EO6(−). Data are from four separate experiments.

(B) Increase in IL-6 from baseline (control) in lung tissue macrophages isolated from WT, *tlr4*$^{-/-}$, *myd88*$^{-/-}$, and *trif*$^{-/-}$ mice in response to LPS (1 ng/ml) or OxPAPC (10 μg/ml). *$p < 0.05$ comparing OxPAPC-treated WT or *myd88*$^{-/-}$ macrophages ± EO6. **$p < 0.01$ compared to OxPAPC EO6(−) treated WT macrophages. Data are from three separate experiments.

(C) Lung elastance in WT mice following intratracheal administration of PAPC or OxPAPC (20 μg/g body weight). n = 4 for each group. **$p < 0.01$ for the whole time course.

(D) Western blots of IκBα and β-actin in lungs isolated from mice 90 min after saline treatment (control), OxPAPC, or PAPC (20 μg/g body weight). Blots are representative of three separate experiments.

(E) Lung elastance at 1.5 hr in WT, *tlr4*$^{-/-}$, *myd88*$^{-/-}$, and *trif*$^{-/-}$ mice following OxPAPC challenge (20 μg/g body weight). The correct genetic background controls are shown. n = 4 for each group. *$p < 0.05$. Data are mean values ± SEM.

could still trigger IL-6 production in *myd88*$^{-/-}$ lung tissue macrophages. LPS-induced IL-6 production in lung macrophages was dependent on TLR4, TRIF, and MyD88 (Figure 4B). In addition, OxPAPC induced higher IL-6 production than nonoxidized PAPC in alveolar macrophages isolated by lung lavage (Figure S8B). OxPAPC-induced IL-6 production was decreased in *tlr4*$^{-/-}$ alveolar macrophages (Figure S8C). Similar to lung macrophages, OxPAPC triggered IL-6 production in peritoneal macrophages dependent on TLR4 and TRIF but not MyD88 (Figure S8D). Thus, OxPAPC can trigger IL-6 production in lung and peritoneal macrophages via TLR4-TRIF signaling. Importantly, intratracheal administration of OxPAPC induced marked deterioration of lung function in WT mice (Figure 4C). In vivo OxPAPC, but not PAPC, challenges triggered IκBα degradation indicative of an activated NF-κB pathway (Figure 4D). Moreover, lung function (Figure 4E) and IL-6 production (Figure S8E) were markedly alleviated in *tlr4*$^{-/-}$ and *trif*$^{-/-}$ but not *myd88*$^{-/-}$ mice. These data indicate that OxPAPC can trigger ALI via TLR4 and TRIF.

Inactivated H5N1 Avian Influenza Virus Can Induce OxPL and ALI in Mice

Patients who died of H5N1 avian influenza or Spanish influenza developed ARDS, and extremely high levels of cytokines have been observed in patients and animals infected with these viruses (Beigel et al., 2005; Tumpey et al., 2005). Our data so far showed that acid aspiration triggers production of OxPLs that can augment the severity of ALI and cytokine production via

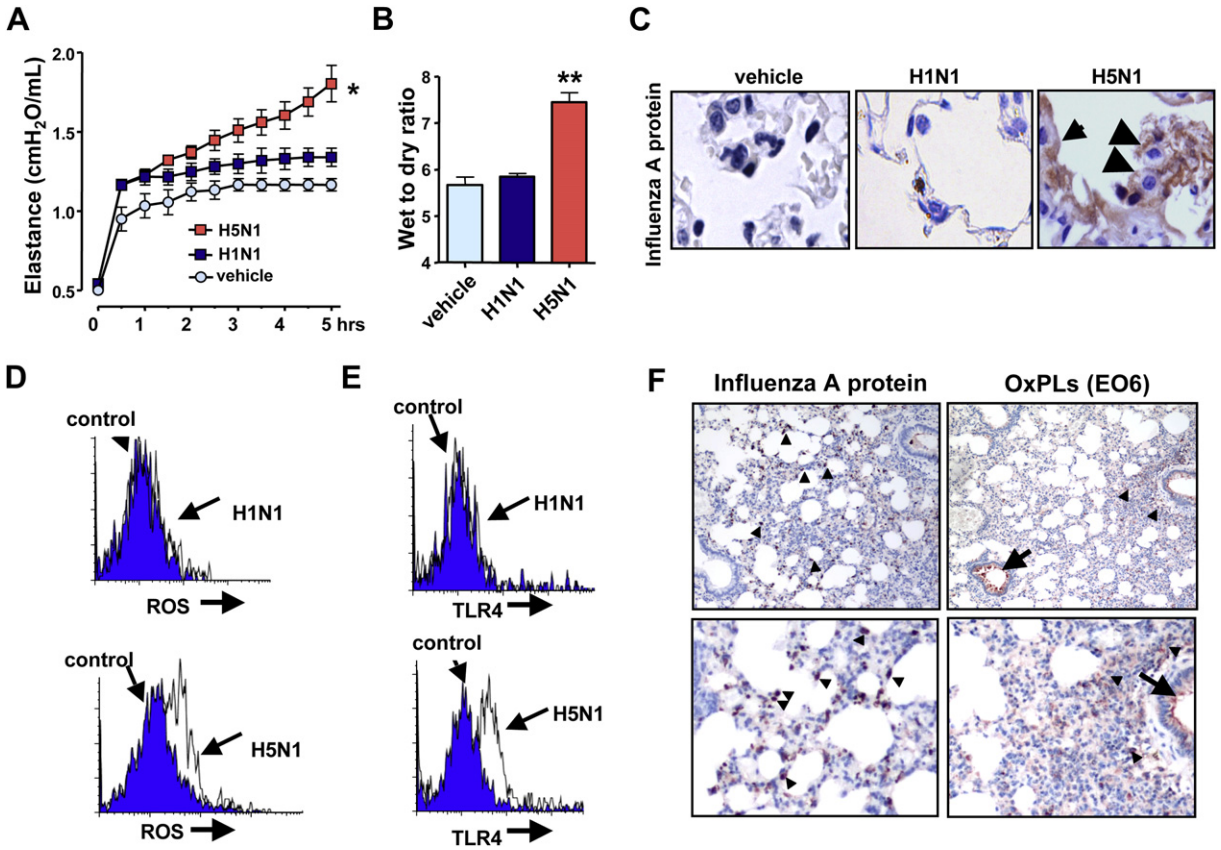

Figure 5. Inactivated H5N1 Avian Influenza Virus Can Induce OxPLs and ALI in Mice

(A) Changes in lung elastance in WT mice following intratracheal administration of vehicle (n = 3), inactivated H1N1 (n = 6), or inactivated H5N1 (n = 8) viruses. *$p < 0.05$ for the whole time course.

(B) Lung edema formation 5 hr after vehicle, inactivated H1N1, or inactivated H5N1 treatment. **$p < 0.01$.

(C) Immunohistochemistry for influenza A nucleoprotein in lung of WT mice challenged with vehicle, inactivated H1N1, or inactivated H5N1 viruses. Influenza A protein-positive cells were present in the lower respiratory tract including alveolar macrophage (arrowhead) and pneumocytes (arrows). Original magnifications × 400.

(D) ROS expression in alveolar macrophages from WT mice treated with control vehicle (blue), inactivated H1N1 virus (white, upper panel), or inactivated H5N1 virus (white, lower panel).

(E) TLR4 expression in alveolar macrophages from WT mice treated with vehicle (blue), inactivated H1N1 virus (white), or inactivated H5N1 virus (white). Representative histograms are shown for five separate experiments. Data in (D) and (E) are at 1 hr after viral challenge.

(F) Immunohistochemistry for influenza A nucleoprotein and EO6-detectable OxPLs in lung of WT mice infected with live H5N1 avian influenza virus. H5N1-infected mice contain large numbers of influenza A protein-positive cells (brown) in the lower respiratory tract (left panels, arrowheads). OxPLs were localized to inflammatory cells (arrowheads) as well as inflammatory exudates (arrow). Lungs were analyzed 4 days after infection. Original magnifications × 100 (upper panels) and × 200 (lower panels). Data are mean values ± SEM.

TLR4. We wanted to extend these findings to H5N1-mediated ALI. Inactivated influenza A virus (McKinney et al., 2003) or inactivated respiratory syncytial virus (Haeberle et al., 2002) can induce rapid activation of NF-κB and/or proinflammatory cytokine production in macrophages. The virulence of the 1918 Spanish influenza virus was largely determined by its hemaglutinin (HA), and the recombinant viruses expressing the 1918 viral HA induce high IL-6 production and severe ALI in vivo (Kobasa et al., 2004). Based on these reports, we tested whether an inactivated H5N1 virus where HA activity is conserved might induce OxPL production and ALI in vivo via TLR4. Since H5N1 subtype influenza A viruses are more potent inducers of cytokines in macrophages than H1N1 subtype influenza (Cheung et al., 2002), we used H1N1 as a control.

Pulmonary challenge of inactivated H5N1 avian influenza virus induced rapid impairment of lung function as determined by increased lung elastance (Figure 5A), severe edema formation as assessed by wet/dry lung weight ratios (Figure 5B), and pathological changes such as alveolar wall thickening, bleeding, or the accumulation of inflammatory cells (Figure S9A). Administration of inactivated H1N1 virus had only very mild effects on lung function and lung histology (Figures 5A, 5B, and S9A). In line with a previous study (van Riel et al., 2006), we observed influenza A virus nuclear protein-positive cells in the lower respiratory tract (LRT) in mice treated with inactivated H5N1 virus (Figure 5C). By contrast, we only found very few virus nuclear protein-positive cells in the LRT of H1N1-treated mice (Figure 5C). Similar to acid treatment, we found higher production of ROS in alveolar

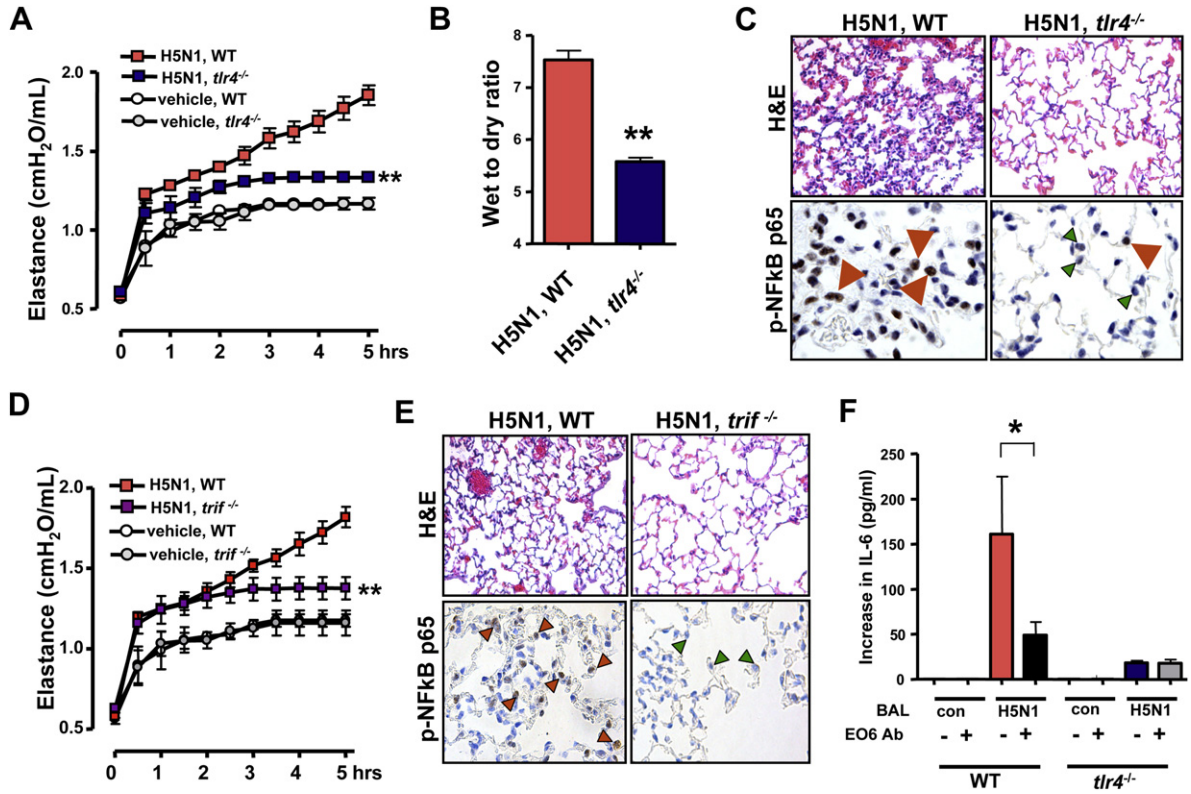

Figure 6. TLR4- or TRIF-Deficient Mice Show Less Severe ALI to Challenge with Inactivated H5N1 Avian Influenza Virus

(A) Lung elastance in WT and *tlr4*$^{-/-}$ mice following administration of vehicle or inactivated H5N1 viruses. n = 5 for each group. **p < 0.01 for the whole time course.

(B) Lung edema formation in WT versus *tlr4*$^{-/-}$ mice 5 hr after H5N1 challenge. **p < 0.01.

(C) Lung pathology (top; H&E staining) and immunolocalization of NFκBp65 (bottom) in lung tissue of H5N1-challenged WT and *tlr4*$^{-/-}$ mice. Note nuclear accumulation of Ser276-phosphorylated NFκBp65 in macrophages from WT lung (red arrows). In H5N1-treated *tlr4*$^{-/-}$ lungs, nuclear NF-κB accumulation was mostly absent from macrophages (green arrows) albeit present in a few cells (red arrow). Original magnifications × 400.

(D) Lung elastance in WT and *trif*$^{-/-}$ mice after administration of vehicle or inactivated H5N1 viruses. n = 5 for each group. **p < 0.01 for the whole time course.

(E) Lung pathology (top; H&E staining) and immunolocalization of NFκBp65 (bottom) in lung tissue of H5N1-challenged WT and *trif*$^{-/-}$ mice. Original magnifications × 400.

(F) BAL fluid from WT mice 5 hr after a H5N1 challenge (BAL H5N1) triggers IL-6 in WT but not *tlr4*$^{-/-}$ alveolar macrophages. BAL fluid from H5N1-treated mice plus an isotype-matched control mAb (–) was compared to BAL fluid from H5N1-treated mice plus the mAb EO6 (+). *p < 0.05. Data are mean values ± SEM.

macrophages isolated from mice treated with inactivated H5N1 avian influenza virus (Figure 5D). In addition, TLR4 surface expression was increased in alveolar macrophages from mice treated with inactivated H5N1 (Figure 5E). In vivo challenge of mice with H1N1 did not result in detectable ROS production or upregulation of TLR4 cell-surface expression (Figures 5D and 5E). Moreover, we detected OxPLs in the BAL fluid of animals challenged with inactivated H5N1 (Figure S9B). Immunohistochemistry confirmed enhanced generation of EO6-detectable OxPLs at the sites of injury (Figure S9C). We extended the analysis of OxPLs to live H5N1 infections. Similar to inactivated H5N1 (Figure 5C), influenza virus A protein was detected in the LRT of mice infected with live H5N1 avian influenza virus (Figure 5F). Importantly, infection with live H5N1 avian influenza virus resulted in the formation of EO6-detectable OxPLs in mouse lung (Figure 5F). Thus, challenge of mice with H5N1 avian influenza can trigger OxPLs and rapid onset ALI in vivo.

Inactivated H5N1-Induced ALI Is Attenuated in *tlr4* and *trif* Mutant Mice

To test whether pulmonary exposure of inactivated H5N1 viruses affects the severity of ALI via the TLR4-TRIF pathway, we analyzed ALI in *tlr4*$^{-/-}$ and *trif*$^{-/-}$ mice. The *tlr4*$^{-/-}$ mice, treated with the inactivated H5N1 virus, showed significantly improved lung elastance (Figure 6A), pulmonary edema formation (Figure 6B), and alleviated lung pathologies (Figure 6C) compared with control WT mice. Moreover, *trif*$^{-/-}$ mice, treated with the inactivated H5N1 virus, showed improved lung elastance (Figure 6D), pulmonary edema formation (Figure S9D), and alleviated lung pathologies (Figure 6E). NF-κBp65 activation in macrophages was also impaired in lungs from *tlr4*$^{-/-}$ and *trif*$^{-/-}$ mice (Figures 6C and 6E,). In addition, BAL fluid obtained from H5N1-challenged mice induced high levels of IL-6 in WT but not *tlr4*$^{-/-}$ alveolar macrophages. Neutralization of OxPLs using the mAb EO6 attenuated IL-6 production in WT but not *tlr4*$^{-/-}$

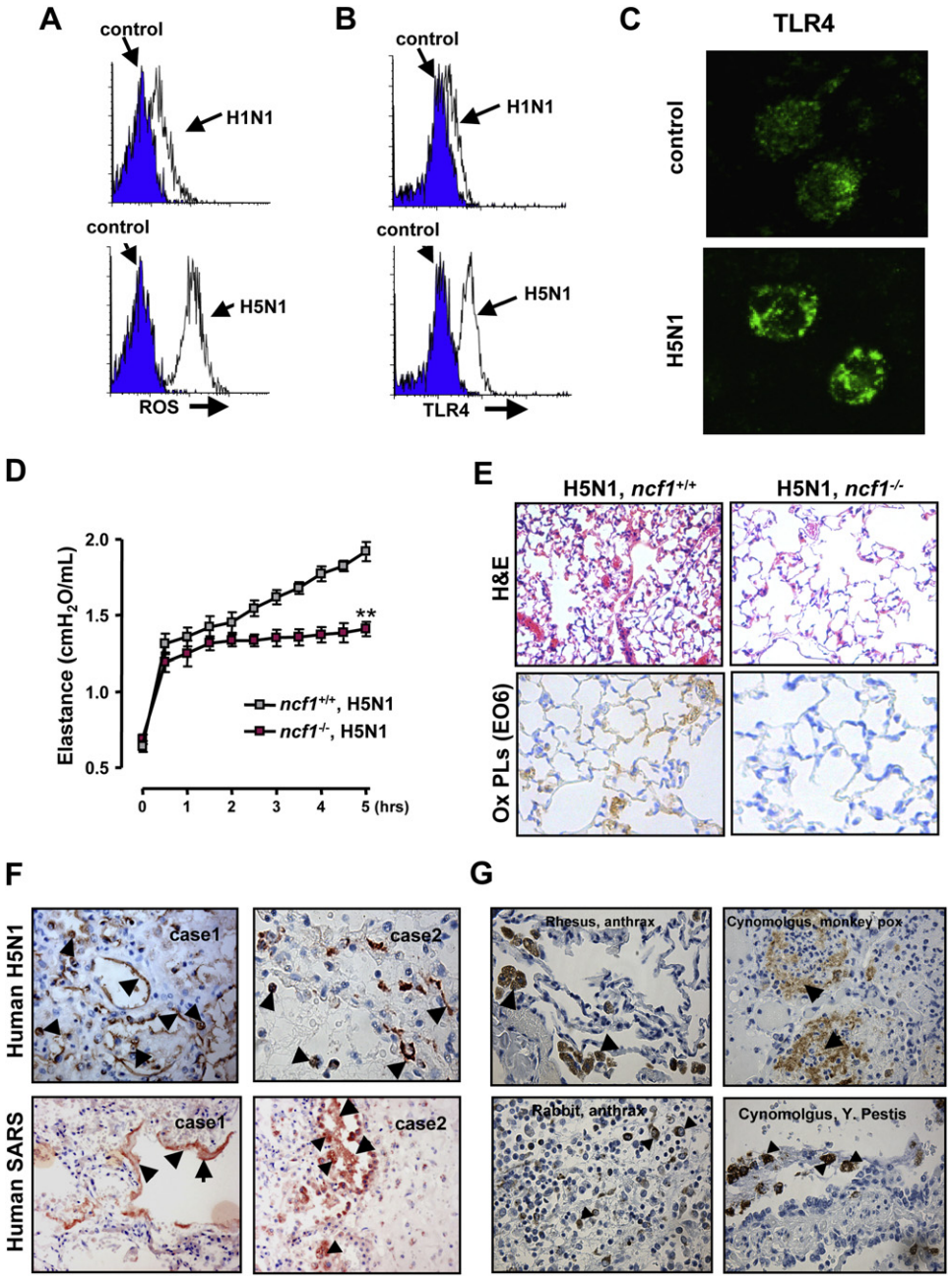

Figure 7. The Oxidative Stress Machinery Controls the Severity of ALI in Response to Inactivated H5N1 Avian Influenza Viruses

(A) ROS expression in control PBMCs and PBMCs from the same donor treated with inactivated H1N1 or inactivated H5N1 viruses. Data are from $CD14^+$ gated PBMCs. Representative histograms are shown for six separate donors.

(B) TLR4 expression in control human PBMCs and H5N1- or H1N1-treated PBMCs. Data are from $CD14^+$ gated PBMCs. Representative histograms are shown for six different donors.

(C) Immunofluorescence staining of TLR4 in PBMCs treated with formulation control or inactivated H5N1. TLR4 was distributed throughout the cytoplasm in control cells (top). PBMCs treated with inactivated H5N1 showed peripheralization of TLR4 (bottom).

(D) Lung elastance in WT and $ncf1^{-/-}$ mice following intratracheal administration of inactivated H5N1 viruses. n = 4 for each group. $^{**}p < 0.01$ for the whole time course.

(E) Lung pathology (top; H&E staining) and immunolocalization of oxidized PLs (bottom) in lung tissue of H5N1-challenged WT and $ncf1^{-/-}$ mice. Original magnifications × 200.

(F) Immunohistochemistry of OxPLs in lungs from two patients infected with H5N1 avian influenza virus (top) and two patients infected with SARS-coronavirus (bottom).

alveolar macrophages (Figure 6F). Thus, cytokine production in alveolar macrophages and ALI in vivo are attenuated in *tlr4* and *trif* mutant mice in response to challenge with inactivated H5N1 avian influenza virus.

H5N1 Avian Influenza Virus Triggers Oxidative Stress in Humans

Next, we examined whether inactivated H5N1 avian influenza viruses can also trigger the oxidative stress machinery in humans. Stimulation of peripheral blood mononuclear cells (PBMCs) with inactivated H5N1 viruses indeed resulted in generation of ROS (Figure 7A). By contrast, challenge with inactivated H1N1 resulted in much less ROS production in human PBMCs. Moreover, FACS staining showed that TLR4 surface expression was upregulated in PBMCs treated with inactivated H5N1 compared to H1N1 (Figures 7B and S10A). Whereas TLR4 protein is distributed throughout the cytoplasm in human PBMCs under control conditions, challenge of PBMCs with inactivated H5N1 virus induced relocalization and cell membrane association of TLR4 (Figure 7C). Thus, inactivated H5N1 viruses can induce ROS formation and TLR4 surface expression on primary human monocytes.

Loss of NCF1 Improves the Severity of ALI

Our data so far showed that inactivated H5N1 viruses can trigger ROS formation in mouse alveolar macrophages and human monocytes. We therefore want to test whether such ROS generation is indeed involved in disease pathogenesis of H5N1 influenza virus-mediated ALI. To address this, we analyzed lung injury in WT and *ncf1* (neutrophil cytosolic factor 1) mutant mice (Hultqvist et al., 2004). Ncf1 is a key component of the NADPH oxidase complex required for oxidative burst and ROS formation (Hultqvist et al., 2004). This *ncf1* mutation affects splicing leading to a near absence of Ncf1 protein (Huang et al., 2000). Interestingly, the *ncf1* mutant mice treated with inactivated H5N1 virus showed significantly improved lung elastance (Figure 7D), pulmonary edema formation (Figure S10B), and alleviated lung pathologies (Figure 7E) compared with control mice on the same genetic background. Importantly, in H5N1-challenged $ncf1^{-/-}$ mice we failed to detect oxidized PL formation (Figure 7E). Thus, genetic impairment of ROS production results in reduced formation of OxPLs and significantly improved lung functions in response to H5N1 challenge.

Multiple Lethal Lung Pathogens Trigger Formation of OxPLs in Different Species

Finally, to test whether OxPLs are generated during actual H5N1 influenza virus infections in humans, we analyzed lung samples from two patients who had developed ARDS following H5N1 avian influenza virus infections. Consistent with our mouse acid aspiration and H5N1 models, we detected massive formation of OxPLs localized at the inflammatory exudates lining the injured air spaces as well as alveolar macrophages in the lungs of both H5N1-infected patients (Figure 7F). Lungs from patients that died of extrapulmonary diseases did not show any detectable OxPL formation (Figure S10C). Thus, H5N1 infections in humans result in the local activation of the oxidative stress machinery and OxPL formation in the lung.

To examine whether OxPL production is a general feature of lethal lung injury that can be seen in different pathogen infections and across wider species barriers, we analyzed lung samples from nine individuals who had developed ARDS following SARS infections. In all SARS-infected human cases tested, we observed marked production of OxPLs in the inflammatory exudates lining the injured air spaces, pneumocytes, as well as alveolar macrophages (Figure 7F and data not shown). To extend these findings to additional species and pathogens, we analyzed lung samples from animals infected with potential bioterrorism agents. We observed formation of OxPLs in Anthrax-infected Rhesus monkeys, Anthrax-infected rabbits, Monkey Pox-infected Cynomolgus monkeys (Macaca fascicularis), as well as Yersinia pestis-infected Cynomolgus monkeys that developed lung plague (Figure 7G). By contrast, we could not detect elevated OxPLs in Smallpox or Marburg virus-infected Cynomolgus monkeys, nor in monkeys infected with Western Equine Encephalitis (WEE) or Eastern Equine Encephalitis (EEE) viruses, diseases that did not cause severe lung injury (data not shown). Thus, in multiple species, infections with various lethal lung pathogens such as H5N1 avian influenza virus, SARS-coronavirus, Anthrax, Y. pestis, or Monkey Pox virus can trigger formation of OxPLs in the lung. These results should be extended to additional pathogens and species.

DISCUSSION

Stimulation of TLR4 can trigger the activation of two downstream signaling pathways: MyD88-dependent or TRIF-dependent pathways (Akira et al., 2006). In the classical pathway, MyD88 recruits IL-1R-associated kinase (IRAK) and TRAF6 leading to activation of IKK$\alpha/\beta/\gamma$ complexes. TRIF signals through IKK-ε leading to activation of IRF3 and the expression of IFN-inducible genes. It has been shown that TRAF6 binds to TRIF though TRAF6-binding motifs in the N-terminal portion of TRIF and is involved in TRIF-mediated activation of NF-κB in vitro (Sato et al., 2003). Importantly, our study shows that innate immune signaling via TLR4-TRIF-TRAF6 is a key genetic pathway that determines the susceptibility to acute lung failure in vivo. Moreover, our bone marrow transplantation experiments and our LysCre TFAF6 mutant mice show that this pathway operates in myeloid cells, in particular lung macrophages. Since macrophages can utilize both TRIF- and MyD88-dependent pathways for cytokine induction, our data might provide an opportunity to minimize ALI via TRIF inhibition while not affecting MyD88-dependent innate immune functions.

Lung has a large surface area that is exposed to the aerobic environment and thus is a highly susceptible site for oxidative events, making the lipids at the air-liquid interface an "ideal" substrate for such lipid modifications. Recently oxidized moieties,

(G) Immunohistochemistry of OxPLs in rhesus monkeys and rabbits infected with Bacillus anthracis (left panels) and Cynomolgus monkeys infected with Monkey Pox or Yersinia pestis (right). In (F) and (G), OxPLs detected by the mAb EO6 were seen in inflammatory exudates lining the injured alveoli (arrows) and macrophages (triangles). Original magnifications × 400. Data are mean values ± SEM.

including OxPLs, have been implicated as pathogen-associated molecular patterns that are detected by several conserved pattern-recognition receptors (Binder et al., 2002; Miller et al., 2003b). In particular, minimally oxidized LDL has been found to activate TLR4 on macrophages (Miller et al., 2003a, 2005), though the exact mechanism of this activation remains elusive. However, this connection has been controversial (Bochkov et al., 2002). We therefore used a genetic approach to examine whether TLR4 expression is indeed required for OxPL-induced cytokine production in macrophages in vitro or OxPL-induced ALI in vivo. Our genetic data show that OxPL-mediated cytokine release and OxPL-induced ALI depend on TLR4 expression. Thus, OxPLs can either directly or indirectly activate the TLR4 signaling cascade during the course of lung injury. Consistent with previous reports (Powers et al., 2006; Kurt-Jones et al., 2000), we also found that chemical injury and inactivated H5N1 virus upregulate TLR4 surface expression in macrophages. Thus, local lung injury not only triggers activation of the oxidative stress machinery but also induces upregulation of TLR4 involved in the OxPL-induced acute lung injury response.

We have identified OxPAPC as an important trigger of ALI. In fact, OxPAPC has been known to be generated at the sites of inflammation and is found in membranes of apoptotic cells (Chang et al., 2004). Furthermore, OxPAPC can play a proinflammatory role in atherosclerosis (Berliner and Watson, 2005; Furnkranz et al., 2005) and impairs the outcome of gram-negative sepsis in vivo (Knapp et al., 2007). Interestingly, in the *E. coli*-induced peritonitis model, coadministration of OxPAPC also increased the local production of cytokines, e.g., IL-6 (Knapp et al., 2007). On the other hand, anti-inflammatory properties of OxPAPC have been reported in LPS-induced sepsis or ALI, which may be explained by direct antagonism of LPS recognition (Bochkov et al., 2002; Nonas et al., 2006). Besides OxPAPC, other OxPLs might also trigger ALI. Moreover, additional TLR4 ligands are also likely to be present, e.g., modified matrix components, dying cells, hyaluronan, or HMGB1 (Miyake, 2007).

One key question remained, whether oxidative stress is indeed involved in disease pathogenesis of ALI. Our data showed that acid treatment and inactivated H5N1 viruses can trigger ROS formation in mouse alveolar macrophages and human monocytes. Oxidative modifications are also present in all severe lung injuries in all species tested. Of note, gene expression analysis of mice infected with recombinant viruses expressing the 1918 viral HA revealed a high upregulation of ROS-related genes (Kash et al., 2004). We therefore tested H5N1-induced lung injury in *ncf1* mutant mice. Ncf1 encodes one of the activating proteins in the phagocytic NADPH oxidase complex. Importantly, this genetic defect in ROS production resulted in a significantly reduced lung injury in response to challenge with our inactivated H5N1 virus. Moreover, in H5N1-challenged *ncf1* mutant mice we failed to observe EO6-detectable oxidized PLs confirming that Ncf1-regulated oxidative burst is involved in the formation of OxPLs. Thus, activation of the oxidative stress machinery is not simply a by-product of the disease process but controls disease severity.

Our results in two experimental ALI models, acid aspiration and inactivated H5N1-induced ALI, indicate that chemical as well as viral lung pathogens trigger the oxidative stress machinery resulting in ROS generation and the local production of OxPLs. Massive formation of OxPLs occurred in all severe cases of acute lung failure we have analyzed including humans who died of H5N1 or SARS infections and animals that developed lethal lung failure due to Y. pestis, Monkey Pox, pulmonary Anthrax, or H5N1 infections. OxPLs such as OxPAPC can directly trigger cytokine production in macrophages and modulate the severity of acute lung injury in vivo dependent on TLR4-TRIF-TRAF6 expression. Thus, the acute onset of proinflammatory immune responses and severe lung injury caused by different pathogens critically depends on activation of the oxidative stress machinery that couples to innate immunity (Figure S11). Modulation of this injury pathway, therefore, could be utilized to protect patients infected with H5N1 avian influenza virus, SARS-coronavirus, Anthrax, or other as yet unknown lethal lung pathogens from developing acute severe lung failure.

EXPERIMENTAL PROCEDURES

For detailed Experimental Procedures see the Supplemental Data.

Clinical Patient Profiles

Lung samples from two H5N1- and nine SARS-infected humans were used.

Animal Infections

C57BL6 mice were infected intranasally with live H5N1 avian influenza virus (strain A/HK/483/97) and euthanized for tissue sampling on day 4. Lethal lung infections with Anthrax, Y. pestis, and Monkey Pox virus, as well as infections with Smallpox virus, Marburg virus, WEE, and EEE and lung sampling were performed at the US Army Medical Research Institute of Infectious Diseases.

Mutant Mice

tlr4, tlr9, myd88, *tlr3, trif*, *irf3*, *il-6,* and *ncf1* mutant mice have been previously described. Mice harboring a floxed TRAF6 allele will be reported in the future and were crossed onto LysCre mice (Clausen et al., 1999). Only sex-, age-, and background-matched mice were used. Basal lung function and lung structure were comparable among all the mice tested.

Acid Aspiration-Induced ALI in Mice

After intratracheal instillation of HCl (pH = 1.5; 2 ml/kg), animals were ventilated for 3 hr. Total positive end expiratory pressure ($PEEP_t$) and plateau pressure (P_{plat}) were measured at the end of expiratory and inspiratory occlusion. Elastance was calculated as ($P_{plat} - PEEP_t$) divided by tidal volume (V_T) every 30 min during the ventilation periods.

Bone Marrow Transplantation

Recipient mice were irradiated and 1×10^6 donor bone marrow cells were delivered i.v. through the tail vein. Chimeras were used for experiments 12 weeks after transplantation.

Preparation of Oxidized Surfactant PLs and In Vivo Treatments

In vitro oxidation of surfactant PLs was performed according to previously established conditions (Rodriguez Capote et al., 2003). The in vivo impact of nonoxidized surfactant PLs and oxidized surfactant PLs was tested in normal, healthy lung as well as saline-lavaged lungs to remove surfactant.

Polymyxin B, LPS, and OxPAPC Treatment in Mice In Vivo

To neutralize LPS, mice received polymyxin B or control vehicle intratracheally. LPS (*E. coli* O111:B4; 0.5 μg/g body weight), OxPAPC (20 μg/g body weight), or control PAPC (20 μg/g body weight) were instilled intratracheally. Animals were then ventilated for 3 hr and pulmonary elastance determined.

H5N1 Avian Influenza Isolates and H5N1-Induced Lung Injury in Mice

Inactivated avian influenza subtypes (H1N1 and A/ck/Yamaguchi/7/04 H5N1) were obtained from the Istituto Zooprofilattico Sperimentale delle Venezie.

Vehicle and inactivated H1N1 or H5N1 viruses were instilled intratracheally. Animals were then ventilated for 5 hr and elastance was calculated every 30 min.

Assessment of Blood Oxygenation and Pulmonary Edema

Partial pressure of arterial oxygen (PaO_2) was measured to assess arterial blood oxygenation as an indicator for respiratory failure. To assess pulmonary edemas, the lung wet/dry weight ratios were calculated.

Histology, In Situ NF-κB Detection, and Immunohistochemistry

Lung tissue was fixed in 4% buffered formalin. For histological analysis, sections were stained with hematoxylin and eosin (H&E). For detection of activated NFκB, paraffin sections were incubated with a polyclonal anti-phospho-NFκBp65 (Ser276) antibody. Immunohistochemistry to detect oxidized phospholipids (OxPLs) was performed using the mAb EO6 (kindly provided by J.L. Witztum). Immunohistochemistry for influenza A virus nucleoprotein was performed using the HB 65 (EVL anti-influenza NP, subtype A) antibody.

Multiple Cytokine Expression Analyses and Cytokine ELISA

Frozen lung tissues were homogenized in cell lysis buffer, and supernatants were assayed using multiplex cytokine arrays. For ELISA analyses, supernatants of homogenized lung tissue were assayed using specific kits.

Isolation and Activation of Macrophages

Bone marrow macrophages were isolated from femurs of 8- to 10-week-old mice. Peritoneal macrophages were obtained by injecting mice with thioglycollate, followed by peritoneal lavage. Alveolar macrophages were obtained from mice by bronchoalveolar lavage (BAL). Lung tissue macrophages were prepared using collagenase and DNase. For measurement of IL-6, macrophages were plated on 96-well plates and stimulated in vitro for 24 hr.

Detection of ROS and TLR4

Mouse alveolar macrophages were obtained from mice treated with vehicle, acid, or inactivated H5N1. Human PBMC were isolated with Ficoll-Hypaque and treated with inactivated H5N1 or H1N1 virus. For ROS detection, cells were incubated with DCF. For mouse TLR4 surface staining, cells were double stained for CD11c and TLR4. For human TLR4 detection, cells were double stained for TLR4 and CD14. ROS and TLR4 expression were assessed by FACS. For TLR4 immunolocalization, PBMCs were fixed, permeabilized, and incubated with anti-TLR4.

Statistical Analyses

All data are shown as mean ± standard error of the mean (SEM). Measurements at single time points were analyzed by ANOVA and, if significant, further analyzed by a two-tailed t test. Time courses were analyzed by repeated-measurements (mixed model) ANOVA with Bonferroni post-tests.

SUPPLEMENTAL DATA

Supplemental Data include eleven figures, Supplemental Experimental Procedures, and Supplemental References and can be found with this article online at http://www.cell.com/cgi/content/full/133/2/235/DC1/.

ACKNOWLEDGMENTS

We thank all members of our laboratories for helpful discussions and critical reading of the paper. We thank Tada Taniguchi for providing IRF3 mutant mice and V. Komnenovic for immunostaining. We are particularly grateful to Fred Possmeyer, Ernst Malle, Juergen Arnold, and Holger Spalteholz for key advice and cooperation. We also thank Hongliang Wang, Haolin Liu, Kangtai Liu, Shunxin Wang, Yang Sun, Ping Ma, Shuan Rao, Feng Guo, and Peng Yang for help with cloning of the recombinant H5 protein and human PBMC work. In addition, we thank LL Pitt and USAMRIID pathology for providing specimens for this study and DTRA as S.B.'s funding agency. J.M.P. is supported by IMBA, the Austrian National Bank, and the Austrian Ministry of Science and Education. Y.I. and K.K. are supported by an EU network grant (EuGenHeart). K.K. and G.v.L. were supported by Marie-Curie Fellowships. Work in the lab of M.P. was supported by EMBL and by grants from the European Union (LSHG-CT-2005-005203 and CT04-005632). M.K. is supported by SNF grant # 3100A0-100233/1. A.S. is supported by the Canadian Institutes of Health Research (CIHR) and the Canada Foundation for Innovation (CFI). This work was also funded by National Natural Science Foundation of China (30421003, 30528002, 30625013, and 30623009) and Ministry of Science and Technology of China (2006AA02Z152 and 2005CB523000).

Received: April 25, 2007
Revised: December 10, 2007
Accepted: February 29, 2008
Published: April 17, 2008

REFERENCES

Adachi, O., Kawai, T., Takeda, K., Matsumoto, M., Tsutsui, H., Sakagami, M., Nakanishi, K., and Akira, S. (1998). Targeted disruption of the MyD88 gene results in loss of IL-1- and IL-18-mediated function. Immunity *9*, 143–150.

Akira, S., Uematsu, S., and Takeuchi, O. (2006). Pathogen recognition and innate immunity. Cell *124*, 783–801.

Bailey, T.C., Da Silva, K.A., Lewis, J.F., Rodriguez-Capote, K., Possmayer, F., and Veldhuizen, R.A. (2004). Physiological and inflammatory response to instillation of an oxidized surfactant in a rat model of surfactant deficiency. J. Appl. Physiol. *96*, 1674–1680.

Beigel, J.H., Farrar, J., Han, A.M., Hayden, F.G., Hyer, R., de Jong, M.D., Lochindarat, S., Nguyen, T.K., Nguyen, T.H., Tran, T.H., et al. (2005). Avian influenza A (H5N1) infection in humans. N. Engl. J. Med. *353*, 1374–1385.

Binder, C.J., Chang, M.K., Shaw, P.X., Miller, Y.I., Hartvigsen, K., Dewan, A., and Witztum, J.L. (2002). Innate and acquired immunity in atherogenesis. Nat. Med. *8*, 1218–1226.

Berliner, J.A., and Watson, A.D. (2005). A role for oxidized phospholipids in atherosclerosis. N. Engl. J. Med. *353*, 9–11.

Bochkov, V.N., Kadl, A., Huber, J., Gruber, F., Binder, B.R., and Leitinger, N. (2002). Protective role of phospholipid oxidation products in endotoxin-induced tissue damage. Nature *419*, 77–81.

Chang, M.K., Binder, C.J., Miller, Y.I., Subbanagounder, G., Silverman, G.J., Berliner, J.A., and Witztum, J.L. (2004). Apoptotic cells with oxidation-specific epitopes are immunogenic and proinflammatory. J. Exp. Med. *200*, 1359–1370.

Cheung, C.Y., Poon, L.L., Lau, A.S., Luk, W., Lau, Y.L., Shortridge, K.F., Gordon, S., Guan, Y., and Peiris, J.S. (2002). Induction of proinflammatory cytokines in human macrophages by influenza A (H5N1) viruses: a mechanism for the unusual severity of human disease? Lancet *360*, 1831–1837.

Clausen, B.E., Burkhardt, C., Reith, W., Renkawitz, R., and Forster, I. (1999). Conditional gene targeting in macrophages and granulocytes using LysMcre mice. Transgenic Res. *8*, 265–277.

Friedman, P., Horkko, S., Steinberg, D., Witztum, J.L., Dennis, E.A., Bird, D.A., Miller, E., Itabe, H., Leitinger, N., Subbanagounder, G., et al. (2002). Correlation of antiphospholipid antibody recognition with the structure of synthetic oxidized phospholipids. Importance of Schiff base formation and aldol condensation. Monoclonal autoantibodies specific for oxidized phospholipids or oxidized phospholipid-protein adducts inhibit macrophage uptake of oxidized low-density lipoproteins. J. Biol. Chem. *277*, 7010–7020.

Furnkranz, A., Schober, A., Bochkov, V.N., Bashtrykov, P., Kronke, G., Kadl, A., Binder, B.R., Weber, C., and Leitinger, N. (2005). Oxidized phospholipids trigger atherogenic inflammation in murine arteries. Arterioscler. Thromb. Vasc. Biol. *25*, 633–638.

Guarner, J., Jernigan, J.A., Shieh, W.J., Tatti, K., Flannagan, L.M., Stephens, D.S., Popovic, T., Ashford, D.A., Perkins, B.A., and Zaki, S.R. (2003). Pathology and pathogenesis of bioterrorism-related inhalational anthrax. Am. J. Pathol. *163*, 701–709.

Haeberle, H.A., Takizawa, R., Casola, A., Brasier, A.R., Dieterich, H.J., Van Rooijen, N., Gatalica, Z., and Garofalo, R.P. (2002). Respiratory syncytial virus-induced activation of nuclear factor-kappaB in the lung involves alveolar macrophages and toll-like receptor 4-dependent pathways. J. Infect. Dis. *186*, 1199–1206.

Hemmi, H., Takeuchi, O., Kawai, T., Kaisho, T., Sato, S., Sanjo, H., Matsumoto, M., Hoshino, K., Wagner, H., Takeda, K., and Akira, S. (2000). A Toll-like receptor recognizes bacterial DNA. Nature *408*, 740–745.

Hoshino, K., Takeuchi, O., Kawai, T., Sanjo, H., Ogawa, T., Takeda, Y., Takeda, K., and Akira, S. (1999). Cutting edge: Toll-like receptor 4 (TLR4)-deficient mice are hyporesponsive to lipopolysaccharide: evidence for TLR4 as the Lps gene product. J. Immunol. *162*, 3749–3752.

Huang, C.K., Zhan, L., Hannigan, M.O., Ai, Y., and Leto, T.L. (2000). P47(phox)-deficient NADPH oxidase defect in neutrophils of diabetic mouse strains, C57BL/6J-m db/db and db/+. J. Leukoc. Biol. *67*, 210–215.

Hudson, L.D., Milberg, J.A., Anardi, D., and Maunder, R.J. (1995). Clinical risks for development of the acute respiratory distress syndrome. Am. J. Respir. Crit. Care Med. *151*, 293–301.

Hultqvist, M., Olofsson, P., Holmberg, J., Backstrom, B.T., Tordsson, J., and Holmdahl, R. (2004). Enhanced autoimmunity, arthritis, and encephalomyelitis in mice with a reduced oxidative burst due to a mutation in the Ncf1 gene. Proc. Natl. Acad. Sci. USA *101*, 12646–12651.

Imai, Y., Kuba, K., Rao, S., Huan, Y., Guo, F., Guan, B., Yang, P., Sarao, R., Wada, T., Leong-Poi, H., et al. (2005). Angiotensin-converting enzyme 2 protects from severe acute lung failure. Nature *436*, 112–116.

Jacobs, D.M., and Morrison, D.C. (1977). Inhibition of the mitogenic response to lipopolysaccharide (LPS) in mouse spleen cells by polymyxin B. J. Immunol. *118*, 21–27.

Kash, J.C., Basler, C.F., Garcia-Sastre, A., Carter, V., Billharz, R., Swayne, D.E., Przygodzki, R.M., Taubenberger, J.K., Katze, M.G., and Tumpey, T.M. (2004). Global host immune response: pathogenesis and transcriptional profiling of type A influenza viruses expressing the hemagglutinin and neuraminidase genes from the 1918 pandemic virus. J. Virol. *78*, 9499–9511.

Knapp, S., Matt, U., Leitinger, N., and van der Poll, T. (2007). Oxidized phospholipids inhibit phagocytosis and impair outcome in gram-negative sepsis in vivo. J. Immunol. *178*, 993–1001.

Kobasa, D., Takada, A., Shinya, K., Hatta, M., Halfmann, P., Theriault, S., Suzuki, H., Nishimura, H., Mitamura, K., Sugaya, N., et al. (2004). Enhanced virulence of influenza A viruses with the haemagglutinin of the 1918 pandemic virus. Nature *431*, 703–707.

Kopf, M., Baumann, H., Freer, G., Freudenberg, M., Lamers, M., Kishimoto, T., Zinkernagel, R., Bluethmann, H., and Kohler, G. (1994). Impaired immune and acute-phase responses in interleukin-6-deficient mice. Nature *368*, 339–342.

Kurt-Jones, E.A., Popova, L., Kwinn, L., Haynes, L.M., Jones, L.P., Tripp, R.A., Walsh, E.E., Freeman, M.W., Golenbock, D.T., Anderson, L.J., and Finberg, R.W. (2000). Pattern recognition receptors TLR4 and CD14 mediate response to respiratory syncytial virus. Nat. Immunol. *1*, 398–401.

Lew, T.W., Kwek, T.K., Tai, D., Earnest, A., Loo, S., Singh, K., Kwan, K.M., Chan, Y., Yim, C.F., Bek, S.L., et al. (2003). Acute respiratory distress syndrome in critically ill patients with severe acute respiratory syndrome. JAMA *290*, 374–380.

Martin, T.R. (1999). Lung cytokines and ARDS: Roger S. Mitchell Lecture. Chest *116*, 2S–8S.

McKinney, L.C., Galliger, S.J., and Lowy, R.J. (2003). Active and inactive influenza virus induction of tumor necrosis factor-alpha and nitric oxide in J774.1 murine macrophages: modulation by interferon-gamma and failure to induce apoptosis. Virus Res. *97*, 117–126.

Michelsen, K.S., Wong, M.H., Shah, P.K., Zhang, W., Yano, J., Doherty, T.M., Akira, S., Rajavashisth, T.B., and Arditi, M. (2004). Lack of Toll-like receptor 4 or myeloid differentiation factor 88 reduces atherosclerosis and alters plaque phenotype in mice deficient in apolipoprotein E. Proc. Natl. Acad. Sci. USA *101*, 10679–10684.

Miller, Y.I., Viriyakosol, S., Binder, C.J., Feramisco, J.R., Kirkland, T.N., and Witztum, J.L. (2003a). Minimally modified LDL binds to CD14, induces macrophage spreading via TLR4/MD-2, and inhibits phagocytosis of apoptotic cells. J. Biol. Chem. *278*, 1561–1568.

Miller, Y.I., Chang, M.K., Binder, C.J., Shaw, P.X., and Witztum, J.L. (2003b). Oxidized low density lipoprotein and innate immune receptors. Curr. Opin. Lipidol. *14*, 437–445.

Miller, Y.I., Viriyakosol, S., Worrall, D.S., Boullier, A., Butler, S., and Witztum, J.L. (2005). Toll-like receptor 4-dependent and -independent cytokine secretion induced by minimally oxidized low-density lipoprotein in macrophages. Arterioscler. Thromb. Vasc. Biol. *25*, 1213–1219.

Miyake, K. (2007). Innate immune sensing of pathogens and danger signals by cell surface Toll-like receptors. Semin. Immunol. *19*, 3–10.

Nagase, T., Uozumi, N., Ishii, S., Kume, K., Izumi, T., Ouchi, Y., and Shimizu, T. (2000). Acute lung injury by sepsis and acid aspiration: a key role for cytosolic phospholipase A2. Nat. Immunol. *1*, 42–46.

Nonas, S., Miller, I., Kawkitinarong, K., Chatchavalvanich, S., Gorshkova, I., Bochkov, V.N., Leitinger, N., Natarajan, V., Garcia, J.G., and Birukov, K.G. (2006). Oxidized phospholipids reduce vascular leak and inflammation in rat model of acute lung injury. Am. J. Respir. Crit. Care Med. *173*, 1130–1138.

Palinski, W., Horkko, S., Miller, E., Steinbrecher, U.P., Powell, H.C., Curtiss, L.K., and Witztum, J.L. (1996). Cloning of monoclonal autoantibodies to epitopes of oxidized lipoproteins from apolipoprotein E-deficient mice. Demonstration of epitopes of oxidized low density lipoprotein in human plasma. J. Clin. Invest. *98*, 800–814.

Peiris, J.S., Yu, W.C., Leung, C.W., Cheung, C.Y., Ng, W.F., Nicholls, J.M., Ng, T.K., Chan, K.H., Lai, S.T., Lim, W.L., et al. (2004). Re-emergence of fatal human influenza A subtype H5N1 disease. Lancet *363*, 617–619.

Poltorak, A., He, X., Smirnova, I., Liu, M.Y., Van Huffel, C., Du, X., Birdwell, D., Alejos, E., Silva, M., Galanos, C., et al. (1998). Defective LPS signaling in C3H/HeJ and C57BL/10ScCr mice: mutations in Tlr4 gene. Science *282*, 2085–2088.

Powers, K.A., Szaszi, K., Khadaroo, R.G., Tawadros, P.S., Marshall, J.C., Kapus, A., and Rotstein, O.D. (2006). Oxidative stress generated by hemorrhagic shock recruits Toll-like receptor 4 to the plasma membrane in macrophages. J. Exp. Med. *203*, 1951–1961.

Rodriguez Capote, K., McCormack, F.X., and Possmayer, F. (2003). Pulmonary surfactant protein A (SP-A) restores the surface properties of surfactant after oxidation by a mechanism that requires the Cys6 interchain disulfide bond and the phospholipid binding domain. J. Biol. Chem. *278*, 20461–20474.

Sato, M., Suemori, H., Hata, N., Asagiri, M., Ogasawara, K., Nakao, K., Nakaya, T., Katsuki, M., Noguchi, S., Tanaka, N., and Taniguchi, T. (2000). Distinct and essential roles of transcription factors IRF-3 and IRF-7 in response to viruses for IFN-alpha/beta gene induction. Immunity *13*, 539–548.

Sato, S., Sugiyama, M., Yamamoto, M., Watanabe, Y., Kawai, T., Takeda, K., and Akira, S. (2003). Toll/IL-1 receptor domain-containing adaptor inducing IFN-beta (TRIF) associates with TNF receptor-associated factor 6 and TANK-binding kinase 1, and activates two distinct transcription factors, NF-kappa B and IFN-regulatory factor-3, in the Toll-like receptor signaling. J. Immunol. *171*, 4304–4310.

Tumpey, T.M., Basler, C.F., Aguilar, P.V., Zeng, H., Solorzano, A., Swayne, D.E., Cox, N.J., Katz, J.M., Taubenberger, J.K., Palese, P., and Garcia-Sastre, A. (2005). Characterization of the reconstructed 1918 Spanish influenza pandemic virus. Science *310*, 77–80.

van Riel, D., Munster, V.J., de Wit, E., Rimmelzwaan, G.F., Fouchier, R.A., Osterhaus, A.D., and Kuiken, T. (2006). H5N1 virus attachment to lower respiratory tract. Science *312*, 399.

Vermeulen, L., De Wilde, G., Notebaert, S., Vanden Berghe, W., and Haegeman, G. (2002). Regulation of the transcriptional activity of the nuclear factor-kappaB p65 subunit. Biochem. Pharmacol. *64*, 963–970.

Veldhuizen, R., Nag, K., Orgeig, S., and Possmayer, F. (1998). The role of lipids in pulmonary surfactant. Biochim. Biophys. Acta *1408*, 90–108.

Ware, L.B., and Matthay, M.A. (2000). The acute respiratory distress syndrome. N. Engl. J. Med. *342*, 1334–1349.

World Health Organization (WHO) (2005). Avian influenza: Assessing the pandemic threat. http://www.who.int/csr/disease/influenza/H5N1-9reduit.pdf.

World Health Organization (WHO) (2008). Sars. http://www.wpro.who.int/health_topics/sars/.

Yamamoto, M., Sato, S., Hemmi, H., Hoshino, K., Kaisho, T., Sanjo, H., Takeuchi, O., Sugiyama, M., Okabe, M., Takeda, K., and Akira, S. (2003). Role of adaptor TRIF in the MyD88-independent toll-like receptor signaling pathway. Science *301*, 640–643.